Geosci. Model Dev. Discuss., 7, 529–562, 2014
www.geosci-model-dev-discuss.net/7/529/2014/
doi:10.5194/gmdd-7-529-2014
© Author(s) 2014. CC Attribution 3.0 License.

Geoscientific Model Development Discussions
Open Access

This discussion paper is/has been under review for the journal Geoscientific Model Development (GMD). Please refer to the corresponding final paper in GMD if available.

A suite of Early Eocene (~ 55 Ma) climate model boundary conditions

N. Herold[1], J. Buzan[2], M. Seton[3], A. Goldner[2], J. A. M. Green[4], R. D. Müller[3], P. Markwick[5], and M. Huber[1,6]

[1]Earth Systems Research Center, Institute for Earth, Ocean and Space Sciences, University of New Hampshire, Durham NH, USA
[2]Department of Earth, Atmosphere, Planetary and Space Sciences, Purdue University, West Lafayette IN, USA
[3]EarthByte Group, School of Geosciences, University of Sydney, Sydney NSW, Australia
[4]School of Ocean Sciences, Bangor University, Menai Bridge, UK
[5]Getech, Leeds, LS8 2LJ, UK
[6]Department of Earth Sciences, University of New Hampshire, Durham NH, USA

Received: 14 December 2013 – Accepted: 18 December 2013 – Published: 17 January 2014

Correspondence to: M. Huber (matthew.huber@unh.edu)

Published by Copernicus Publications on behalf of the European Geosciences Union.

Abstract

We describe a set of Early Eocene (~ 55 Ma) climate model boundary conditions constructed in a self-consistent reference frame and incorporating recent data and methodologies. Given the growing need for uniform experimental design within the Eocene climate modelling community, we make publically available our datasets of Eocene topography, bathymetry, tidal dissipation, vegetation, aerosol distributions and river runoff. Particularly our Eocene topography and bathymetry has been significantly improved compared to previously utilized boundary conditions. Major improvements include the paleogeography of Antarctica, Australia, Europe, the Drake Passage and the Isthmus of Panama, and our boundary conditions include modelled estimates of Eocene aerosol distributions and tidal dissipation for the first time, both consistent with our paleotopography and paleobathymetry. The resolution of our datasets ($1^\circ \times 1^\circ$) is also unprecedented and will facilitate high resolution climate simulations. In light of the inherent uncertainties involved in reconstructing global boundary conditions for past time periods these datasets should be considered as one interpretation of the available data. This paper marks the beginning of a process for reconstructing a set of accurate, open-access Eocene boundary conditions for use in climate models.

1 Introduction

Growth of the paleoclimate modelling community has made it desirable to openly distribute the boundary condition datasets used in published research. This serves two purposes: (1) that effort is not needlessly duplicated between research groups. The construction of input datasets for global climate models takes considerable effort and expertise. Thus, unless scientific disagreement exists, the process need only be conducted once; (2) that inter-model differences result only from variations in internal model assumptions and computational infrastructure. By holding boundary conditions fixed this enables a greater level of scientific understanding of the reasons for

GMDD
7, 529–562, 2014

differences and commonalities between different groups' efforts. This was the impetus for the Paleoclimate Modelling Intercomparison Project (Braconnot et al., 2012), which assesses inter-model variation in Quaternary climate simulations and for which a consistent set of boundary conditions are openly available. Initiatives such as this have successfully fostered collaborations between research groups and provide a baseline for those wishing to conduct Quaternary climate simulations.

An ensemble of opportunity assembled in an ad hoc fashion, designated the Eocene Modelling Intercomparison Project (EoMIP), has already been conducted using climate simulations described in studies published over the past several years (Lunt et al., 2012). Consequently each model in this intercomparison differed at least partially with respect to their prescribed boundary condition forcing. In the spirit of encouraging data consistency within the Eocene climate modelling community we herein document a set of openly available and self-consistent climate model boundary conditions for the Early Eocene (~ 55 Ma). While their intended application is in climate modelling, the broadening domain of geoscientific models may see them applied in a variety of numerical frameworks (e.g. Sect. 2.3). Specifically, this paper describes a newly updated Eocene topography, arguably the most important boundary condition for reconstructing past climates and one with a long history of inquiry in paleoclimate modelling (Donn and Shaw, 1977; Barron et al., 1981). An accompanying dataset of the variation in sub grid cell scale Eocene elevations is also provided. We include a reconstructed Eocene bathymetry, which captures an unprecedented level of detail needed to meet the growing need for reconstructing regional Eocene oceanography (e.g. Hollis et al., 2012). The first estimate of Eocene tidal dissipation (Green and Huber, 2013) is also made available, complementing this recent addition to global climate models' suite of inputs and which may have particular relevance for Eocene climate and oceanography (Lyle, 1997). Eocene vegetation simulated by a dynamic vegetation model is also discussed and provided. Simulated Eocene aerosol distributions are provided – again taking advantage of this recent addition to atmospheric models' prognostic capabilities – to account for the direct effects of Eocene dust, sea salt, sulphate and organic and black

GMDD
7, 529–562, 2014

carbon. Finally, river runoff directions are provided based on the gradient of Eocene topography. All of our datasets are made available at 1° × 1° to facilitate high resolution global and regional simulations.

Previous efforts have been made to assemble self-consistent Eocene boundary conditions (Crowley and Burke, 1998; Sewall et al., 2000) and provide motivation for our work here. While our boundary conditions incorporate more recent data and methodologies than most of those used previously, there are many aspects of Eocene tectonics and climate that remain uncertain or controversial. Thus in many regions our boundary conditions merely reflect one interpretation of the available data and may conflict with alternate interpretations (e.g. the North American Cordillera). Our aim here is not to propose a "correct" set of Eocene boundary conditions but to provide boundary conditions that can enable broader participation by the Eocene climate modelling community as well as greater transparency and reproducibility among groups. Researchers are encouraged to change these datasets based on their own data or interpretations.

2 Reconstructing the Eocene Earth

2.1 Topography

The paleogeographic maps first used in climate modelling (Barron, 1980; Donn and Shaw, 1977) were semi-global in extent and were derived in large by Vinogradov et al. (1967) and Phillips and Forsyth (1972). However, the first global Eocene paleogeographic map applied to a climate model (Barron, 1985) was based on the work of Fred Ziegler and his colleagues at the University of Chicago, who had reconstructed a suite of Mesozoic to Cenozoic paleotopographies (Ziegler et al., 1982). These paleotopographies were built upon and succeeded by Christopher Scotese in the Paleomap Project (Scotese and Golonka, 1992), which was adopted by contemporary modelling efforts (Sloan and Rea, 1996; Sloan, 1994). Almost a decade later, Sewall et al. (2000) published a new global Eocene topography incorporating the latest regional tectonic

GMDD
7, 529–562, 2014

data (Fig. 1a). For over a decade this dataset has remained, without update, a highly utilized topography for Eocene climate modelling (Huber and Caballero, 2011; Winguth et al., 2009; Huber et al., 2003; Shellito et al., 2009; DeConto et al., 2012), and thus a dataset incorporating more recent scholarship is overdue.

Here we adapt the Early Eocene paleotopographic map from Markwick (2007) (Fig. 1b). This map comes from a suite of Cretaceous to modern paleotopgraphies which – similar to the Paleomap project (Scotese and Golonka, 1992) – has its origins in the Paleogeographic Atlas Project at the University of Chicago (Ziegler et al., 1982). Naturally, these maps have been augmented with more recent faunal, floral and lithological data and use a more recent rotation model (Rowley, 1995 unpublished). The primary method used to derive this Eocene topography is based on methods described by Ziegler et al. (1985) and further documented by Markwick (2007), in which contour intervals of 1000 m or less are estimated by comparing past tectonic regimes to their present day analogues. Subsequent to this step adjustments to the paleo shoreline are made based on known Eocene biogeography (see Fig. 39 Markwick, 2007 for a map of known records). Thus, the paleotopographic map of Markwick (2007) consists of a potential range of elevations for each grid cell, instead of an explicit value. A significant benefit of this method over others (e.g. Sewall et al., 2000) is obviation of the need for explicit paleo-elevation estimates – which are scarce for most time periods and regions – while providing an approximate yet quantitative description of topography over a wide area of the Earth. The obvious limitation, however, is the lack of precision and topographic detail away from contour lines, which becomes significant in continental interiors where large anomalous plateaus appear (Fig. 1b).

Climate models require explicit and globally gridded elevation data so a conversion from the vector-based Geographic Information Systems approach underlying the topography of Markwick (2007) to a discrete digital elevation model was necessary. To add detail to regions bounded by contour intervals we apply a tension spline using the contour lines and sea-level as tie points. This creates continuous discrete elevations at all locations. In order to provide plausible peak elevations and gradients

GMDD
7, 529–562, 2014

along known mountain ranges (e.g. the North American and Andean Cordilleras) artificial tie points were added by inserting mountain spines in these areas. The process of interpolation was performed using the cssgrid function (Cubic Spline Sphere Gridder) from the National Center for Atmospheric Research (NCAR) Command Language (UCAR/NCAR/CISL/VETS, 2013) and a constant tension factor of 10.

Additional adjustments were made to conform the topography of Markwick (2007) to more recent or broadly accepted regional paleogeographic reconstructions. The evolution of the Isthmus of Panama is highly debated (Molnar, 2008), primarily due to its potential implications for faunal migration (Iturralde-Vinent, 2006) and ocean circulation (cf. Zhang et al., 2012; Klocker et al., 2005; Lunt et al., 2008). In the Early Eocene it is generally believed to have consisted of a deep gateway between North and South America and thus we base our Panamanian paleogeography on Iturralde-Vincent (2006). We also adopt the new ANTscape Antarctic topographic reconstruction (Wilson et al., 2012) which incorporates, among other improvements, a more elevated West Antarctic bedrock (cf. Fig. 1a and c). Here we have assumed that no significant volume of continental ice existed in the Early Eocene (Cramer et al., 2011). Additional changes include those to Australian (Langford, 2001) and European (Iakovleva et al., 2001; Golonka, 2011; Torsvik et al., 2002) paleogeography.

While our dataset provides global coverage of land elevation there are several regions which suffer from large topographic uncertainty. The south margin of Eurasia is one such area. Prior to India's collision with Eurasia, between 55 and 45 Ma, geological evidence suggests Eurasia's southern margin may have been up to 4 km high (Molnar et al., 2010 and references therein). However, recent thermochronologic and cosmogenic nuclide data indicate relatively low relief persisted prior to collision (Hetzel et al., 2011). Our dataset represents a mean of the proposed uplift histories, with a peak elevation of 1500 m, and thus this is a region that researchers may wish to modify.

The uplift history of North American Cordillera is also subject to debate. Numerous paleoaltimetry measurements based on oxygen isotope geochemistry suggest that western North America was relatively high, on the order of 3–4 km, since the early

GMDD
7, 529–562, 2014

Cenozoic (e.g. Mix et al., 2011). However, other geological records indicate a late Cenozoic uplift (e.g. Stock et al., 2004; Wakabayashi and Sawyer, 2001). Again we choose a somewhat intermediate value between these contrasting uplift histories, and constrain North American topography to approximately 2500 m (Fig. 1c).

Despite the uncertainties which remain in our reconstructed topography, there are several substantial improvements over the reconstruction of Sewall et al. (2000). Firstly, we revise the extent of the Mississippi Embayment, reducing its area in accordance with marine carbonate, coal and peat distributions (Sessa et al., 2012; Markwick, 2007) (Fig. 1). Secondly, the ANTscape Antarctic topography and its rotation are substantially more accurate than that of Sewall et al. (2000), which had an erroneously small Antarctic continental area. Thirdly, the width of the Drake Passage is also reduced in our reconstruction to be more in accordance with data, which imply an extremely nascent gateway. Our final adjusted Eocene topography is shown in Fig. 1c.

Numerous atmospheric processes at the sub grid cell scale have important effects on resolvable processes in global atmospheric models and thus require parameterisation. An important parameter is the variation of topography within each grid cell, which allows models to parameterize atmospheric gravity waves. Global atmospheric circulation models are sensitive to the parameterized wave drag and to their waves. These waves are important for the atmosphere's momentum balance, jet stream strength and the vertical transport of tracers, such as H_2O. In modern simulations the variability of sub grid cell scale topography is represented by the standard deviation of elevations within each model grid cell. For example, the variation of topography in a $1^\circ \times 1^\circ$ model grid cell is calculated from the standard deviation of all elevations within the $1^\circ \times 1^\circ$ domain using a $1' \times 1'$ dataset (e.g. ETOPO1, Amante and Eakin, 2009). However, for past time periods knowledge of surface elevation at such a high resolution is impossible. To overcome this lack of information and provide an estimate of the Eocene variability of sub grid cell scale topography we use the empirical relationship between modern elevation and the standard deviation of sub grid cell scale topography, derived from the

GMDD
7, 529–562, 2014

ETOPO1 dataset (Amante and Eakin, 2009). A script that performs this task on a given topographic dataset is provided in the electronic supplement.

In Fig. 2 we illustrate this process on our $1^\circ \times 1^\circ$ Eocene topography. Firstly, the modern ETOPO1 topography is regridded from its native $1' \times 1'$ resolution to $1^\circ \times 1^\circ$ (Fig. 2a), then, within each 1° x1° grid cell the standard deviation of elevations in the original ETOPO1 dataset are calculated (Fig. 2b). The Greenland and Antarctic ice-sheets are excluded from this process given their smoothness compared to continental crust. Secondly, an array of 100 m bins are created from 0 m to 5500 m – representing the range of modern elevations – and the area-weighted average of the standard deviations of the grid cells that fall within each bin (calculated in the previous step) are calculated, resulting in an array of 55 values (Fig. 2c). Lastly, given the clear monotonic relation between height and standard deviation between sea-level and approximately 3000 m, and between 3000 m and 5500 m, two separate linear regressions are calculated for these intervals (Fig. 2c) to assign estimates of Eocene variability in sub grid cell scale topography to each grid cell (Fig. 2d). Given that the maximum elevation in our Eocene topography is less than 3000 m (Fig. 1c) only the first linear regression is applicable in this paleotopography.

Figure 2c shows a peak in standard deviations of approximately 800 m at elevations between 2500 m and 3500 m. This corresponds to the "Andean-type" environments identified by Ziegler (1985) such as the boundaries of the Tibetan Plateau and Andean Cordillera (Fig. 2b). This broad peak remains regardless of the resolution we downscale ETOPO1 to, though its magnitude and width decreases with increasing resolution. Combined with an adequately derived atmospheric lapse rate, this dataset of sub grid cell scale topographic variability may also be used to constrain uncertainty in surface temperatures simulated by climate models which result from differences in the paleo elevation of a proxy record's site and the elevation resolved in our reconstructed topography (e.g. Huber and Caballero, 2011; Sewall et al., 2000; Sewall and Sloan, 2006).

GMDD
7, 529–562, 2014

2.2 Bathymetry

The first bathymetric maps used for Eocene ocean modelling constituted bowl-like basins in which the oceanic crust was treated primarily as abyssal plain (Barron and Peterson, 1991). The choice of a relatively flat bathymetry, although dictated to some extent by model resolution and available geological data, was informed by the lack of large scale oceanic responses to bathymetric details (Barron and Peterson, 1990). However, this result was misleading due to the lack of treatment of crucial oceanic processes in the models of that generation (e.g. see Sect. 2.3). The most recent Eocene bathymetric datasets include the locations of mid-ocean ridges and shelf slope hypsometry (Bice et al., 1998; Huber et al., 2003). However, given that the highest level of detail in these datasets consisted of only six depth classes and $\sim 3 \times 1.5^{\circ}$ horizontal resolution, substantial gains are to be made by employing new methodologies and higher resolution base datasets to reconstruct Eocene bathymetry.

Here we adapt the global 55 Ma bathymetry of Müller et al. (2008b), which is part of a suite of paleobathymetric maps reconstructed from 140 Ma to the present. Like previous efforts the foundation of this bathymetry is the application of an age–depth relationship to reconstructed seafloor spreading isochrons. As lithospheric crust ages and cools on its path away from the mid-ocean ridge, thinning occurs (Fig. 3a and b). For our chosen Eocene bathymetry the age–depth relationship derived by Stein and Stein (1992) was applied to reconstructed 55 Ma seafloor ages;

$$\text{If } t < 20\,\text{Ma}; \quad d(t) = 2600 + 365t^{1/2}$$

$$\text{If } t \geq 20\,\text{Ma}; \quad d(t) = 5651 - 2473\exp(-0.0278t)$$

where d is the basement depth in meters and t is time in Myr. Several age–depth relationships have been previously tested to determine the best match to modern bathymetry, with Stein and Stein (1992) showing the least bias (Herold et al., 2008; Müller et al., 2008b). To accommodate regions where present day preserved crust is not available for the Eocene (due to the subsequent subduction of oceanic crust)

GMDD
7, 529–562, 2014

symmetric mid-ocean ridge spreading was assumed and seafloor spreading isochrons from the conjugate plate applied. In regions where no data was available from the conjugate plate interpolation was applied between available isochrons and the adjacent plate margin (Müller et al., 2008a, b).

On tectonic time scales (Myrs) the development of Large Igneous Provinces (LIPs) can have significant impacts on global sea-level (Müller et al., 2008b) and ocean circulation (Herold et al., 2012), thus LIPs form an important component of our Eocene bathymetry. These bathymetric features are reconstructed by applying modern LIP outlines and estimating paleo LIP height following Schubert and Sandwell (1989). Additionally, given that certain regions of the modern ocean are covered by sediment up to several kilometres thick (Whittaker et al., 2013) reconstructed sediment thicknesses also represent an important component of reconstructed paleobathymetries. Based on an empirical relationship with age and latitude (polar latitudes generally having larger river runoff and tropical latitudes subject to high marine productivity), an age–latitude relationship was applied (Müller et al., 2008b, Supplement) to reconstruct Eocene sediment thickness (Fig. 3c).

While the methodology adopted from Müller et al. (2008b) represents a substantial improvement over previous bathymetric maps, it is by design a generic process used to reconstruct bathymetry over the past 140 Myr. Therefore discrepancies exist in some regions where paleoceanographic data have been recovered. Particularly, the depths of certain LIPs may be verified against known depth habitats of foraminifera recovered from deep-sea cores. Such a verification was carried out here using Deep Sea Drilling Project and Ocean Drilling Project records. Based on these records the depth of the Madagascar Ridge (Schlich, 1974), Mascarene Ridge (Backman, 1988; Fisher, 1974; Vincent et al., 1974), Shatsky Rise, Ontong Java Plateau (Barrera, 1993), Kerguelen Plateau (Mackensen, 1992), Walvis Ridge (Zachos et al., 2005; Fuetterer, 1984) and the Rio Grande Rise (Perch-Nielsen, 1977) were adjusted.

Reconstructing the tectonic history of ocean gateways is critical in explaining past ocean circulation (Scher and Martin, 2006; Hill et al., 2013), faunal migration patterns

GMDD
7, 529–562, 2014

(Dalziel et al., 2013a) and potentially global climate change (Barker and Thomas, 2004). The Drake Passage and Tasman gateway are of particular significance given their opening was a requirement for development of the Antarctic Circumpolar Current, the largest ocean current in the world (~ 130 Sv) and the only current with a circum global reach (Barker and Thomas, 2004). Unfortunately, the Drake Passage suffers from poor age constraints due to the tectonically complex Scotia arc region and estimates of its opening range from the middle Eocene to late Miocene (cf. Dalziel et al., 2013b; Scher and Martin, 2006). As our bathymetry aims to represent the Early Eocene time period of ~ 55 Ma we prescribe an oceanographically closed Drake Passage, constraining its depth to less than 100 m. Multiple paleoceanographic and tectonic records indicate that the Tasman gateway did not open to deep flow until the late Eocene (Stickley et al., 2004), although when a shallow opening appeared is debatable. Our reconstruction of tectonic plate positions as well as the location of Tasmania suggests a shallow epicontinental sea may have existed and thus we prescribe a depth of 30 m or less in the Tasman gateway. Finally, no data is available for the bathymetry of inland seas or continental shelves in our base datasets and thus we derive their depths by assuming a maximum value of 50 m for inland seas and using a Poisson equation solver to interpolate intermediate values for both areas. Figure 3d shows our final Eocene bathymetry.

The plate rotation model used to construct our paleobathymetry differs from that used for our Eocene topography (Sect. 2.1). To maintain a consistent reference frame between the two datasets we re-rotate our Eocene topography using the plate rotation model of Müller et al. (2008b). This was achieved by changing the reference plate (Africa) location from that determined by Ziegler to that determined by Müller et al. (2008b), resulting in a relative shift of the other continents. Refinements to the location of some continental blocks were made to improve the match between the locations of continental crust in our bathymetry and topography datasets. These steps were largely achieved using the open source software packages GPlates (http://www.gplates.org/), for digitizing polygons, and Generic Mapping

GMDD
7, 529–562, 2014

Tools (http://gmt.soest.hawaii.edu/) for rotating the data. The final merged Eocene topography and bathymetry is shown in Fig. 4 alongside ETOPO1.

2.3 Tidal dissipation

The importance of tidal dissipation in the ocean's general circulation stems from the fact that diapycnal (i.e. vertical) mixing is greatly affected by the tide's interaction with bathymetry. Large increases in diapycnal mixing are observed above regions of rough topography (e.g. Polzin et al., 1997) and are primarily a result of breaking tidally induced internal waves (Garrett and Kunze, 2007; Jayne et al., 2004). Tidal models have been used to predict the amount of tidal energy dissipated in the oceans and to better constrain vertical mixing profiles incorporated in ocean general circulation models (e.g. Simmons et al., 2004). Such experiments have demonstrated that tidal energy considerations significantly reduce the discrepancy between simulated and observed modern ocean heat transport (Simmons et al., 2004) and provides motivation for explicitly including tidal dissipation in past climate simulations (e.g. Green and Huber, 2013; Egbert et al., 2004).

New ocean general circulation models are beginning to incorporate tidal dissipation (e.g. the Community Earth System Model; CESM, Gent et al., 2011). Green and Huber (2013) applied a tidal model using the bathymetry described in Sect. 2.2 and showed that, while total Eocene tidal dissipation was weaker than present, a larger amount of tidal energy was dissipated in the deep ocean, especially in the deep Pacific. The vertical diffusivities associated with these results are significantly larger than present, supporting arguments that enhanced vertical mixing in the Eocene oceans helps to explain the low equator to pole temperature gradient inferred from geological records (e.g. Lyle, 1997), but that have hitherto been difficult to reproduce in models (Lunt et al., 2012).

We distribute the dataset from Green and Huber (2013) here as a map of energy dissipated per unit area (Fig. 5). Models such as the National Center for Atmospheric Research CESM can utilize this dataset to drive their tidal mixing schemes. While this

GMDD
7, 529–562, 2014

work represents a coarse first attempt at deriving Eocene tidal dissipation, to our knowledge no similar effort has been made and thus this dataset provides a baseline for groups who do not have access to the tools required for deriving tidal dissipation. However, given the infancy of this application to deep time paleoclimate it is likely that such a dataset will be improved upon.

2.4 Vegetation

Climate models have long indicated the substantial global and regional effects of vegetation on climate (Otto-Bliesner and Upchurch, 1997; Dutton and Barron, 1997), though newer models indicate a weaker sensitivity (Henrot et al., 2010; Micheels et al., 2007). A series of Tertiary vegetation maps based on paleofloral records (Wolfe, 1985) formed the foundation of many early paleoclimate simulations that explicitly included a paleovegetation boundary condition (e.g. Sloan and Rea, 1996; Dutton and Barron, 1997). Subsequently, Sewall et al. (2000) developed a new Eocene vegetation distribution taking into account more recent data and the effects of a low equator-to-pole temperature gradient. Like their Eocene topography, the vegetation reconstruction of Sewall et al. (2000) has remained highly utilized by the Eocene climate modelling community (e.g. Huber et al., 2003; Liu et al., 2009; Roberts et al., 2009; Huber and Caballero, 2011; Shellito et al., 2003).

We choose to reconstruct Early Eocene vegetation using the offline dynamic vegetation model BIOME4 (Kaplan et al., 2003). For input into BIOME4 we use temperature, precipitation and cloud cover from a CESM simulation forced with the Eocene topography and bathymetry described in Sects. 2.1 and 2.2, respectively, and an atmospheric CO_2 concentration of 2240 ppmv, which has been found to approximately reproduce Eocene temperatures (Huber and Caballero, 2011). This CESM simulation was integrated for 250 yr and initialized with output from a previous CESM simulation that was integrated for over 3000 yr (this latter simulation was forced with the boundary conditions of Sewall et al. (2000) for topography and vegetation, and Huber et al. (2003) for bathymetry, mixed-layer ocean simulations of which are described by Goldner et al.,

GMDD
7, 529–562, 2014

2013). The BIOME4 was forced with a CO_2 concentration of 1120 ppmv since higher concentrations resulted in large scale reductions in tropical forest. Due to the significant differences between modern and Eocene topography (Fig. 4), the anomaly method typically used for specifying input into the BIOME4 (Kaplan et al., 2003) was not possible and thus first order biases in our control CESM simulations are not taken into consideration. However, given that the CESM simulates modern land and sea-surface temperatures broadly consistent with observations (Gent et al., 2011) and that the biases in the modern CESM climate are small in comparison with the simulated change in climate for the Eocene (Huber and Caballero, 2011) we do not believe this to be a significant issue. While asynchronous coupling between our climate and vegetation models precludes the ability of the simulated vegetation to affect climate – as compared to synchronous coupling efforts (e.g. Shellito and Sloan, 2006b, a) – it benefits our results by not erroneously amplifying biases in our climate model (e.g. Wohlfahrt et al., 2008). Figure 6a and b shows the simulated pre-industrial and Eocene distribution of biomes, respectively. For ease of comparison we show these biome maps simplified from the 27 biomes simulated by BIOME4 to 10 mega biomes (derived by Harrison and Prentice, 2003). Our BIOME4 simulated vegetation compares well with vegetation inferred from Paleocene and Eocene palynoflora (Utescher and Mosbrugger, 2007; Morley, 2007) and are consistent with geological indicators of climate (Crowley, 2012). One apparent bias is that an abundance of relatively dry vegetation exists in northern South America according to BIOME4 (cf. Morley, 2007). However, there remains a distinct lack of records for validation from large regions of South Africa and Siberia. We also note that "grass" did not exist at the biome level in the Eocene (Strömberg, 2011), and thus the "Grassland and dry shrubland" biome presented in Fig. 6 should be interpreted as the latter. Our vegetation reconstruction reflects responses to simulated Eocene climate and is therefore less zonal than previous reconstructions (Sewall et al., 2000) while still maintaining efficacy with regard to paleoflora data.

GMDD
7, 529–562, 2014

2.5 Aerosols

Aerosols in Eocene climate simulations have previously been prescribed at pre-industrial levels or set to arbitrarily determined, globally uniform values. Aerosols constitute one of the largest uncertainties in radiative forcing under future anthropogenic greenhouse warming (Stocker et al., 2013) and may be important in resolving some long standing paleoclimate conundrums (Kump and Pollard, 2008). Insufficient proxies from the pre-Quaternary prevent the reconstruction of this boundary condition from geological records. However, the advent of aerosol prognostic capabilities in atmospheric models allows the paleo-distribution of various aerosol species to be simulated (Heavens et al., 2012). Here we again employ the NCAR CESM in a configuration that utilizes the newly implemented Bulk Aerosol Model, which is a component of the Community Atmosphere Model 4 (Neale et al., 2010). In this configuration the model explicitly simulates the monthly horizontal and vertical distribution of dust, sea salt, sulphate, and organic and black carbon aerosols consistent with our Eocene topography (Fig. 7). The Bulk Aerosol Model makes simplistic assumptions regarding the size distribution of aerosol species, compared to the more complicated Modal Aerosol Models. A detailed description of the steps involved in simulating the paleo-distribution of aerosols is provided by Heavens et al. (2012). Here we branch the same CESM simulation described in Sect. 2.4 while also enabling the Bulk Aerosol Model.

Various aerosol species require the specification of emission sources in the Bulk Aerosol Model and this is done in accordance with Heavens et al. (2012). One exception is that we do not specify any volcanic sources of SO_2 or SO_4, given their small radiative effects as well as the uncertainty in the distribution of Eocene volcanoes. Another largely unconstrained yet climatically relevant emission source in the Bulk Aerosol Model is that of dust. In the Bulk Aerosol Model dust is emitted solely from the desert plant functional type which in turn is determined from the prescribed vegetation. It is generally understood that cooler climates promote more dust-laden atmospheres – due to increases in desertification, reduced soil moisture and stronger winds (Bar-Or et al.,

GMDD
7, 529–562, 2014

2008). However, the degree to which global Eocene dust concentrations differed from typical glacial-interglacial variability is uncertain, though regional evidence exists for substantially weak dust fluxes in the early Cenozoic (Janecek and Rea, 1983). Here we have assumed that global Eocene dust loading was approximately three quarters that of the pre-industrial era. The sources of dust in our dataset (i.e. deserts) were manually distributed based loosely on the distribution of Early Eocene evaporites (Crowley, 2012), which itself follows the expected distribution of subtropical high pressure regions. Our chosen concentrations provide an Eocene dust loading intermediate to simulations which prescribe pre-industrial values (e.g. Heinemann et al., 2009; Lunt et al., 2010; Winguth et al., 2009) and those which eliminate the radiative effects of aerosols altogether (Huber and Caballero, 2011). The significant improvement in the approach taken here is that the distribution of aerosols is equilibrated with Eocene geography, providing a realistic regional representation of their radiative forcing.

It is important to stress the large uncertainty in aerosol loading and distribution during past climates and that our simulated concentrations are likely highly model dependant. Furthermore, the aerosol datasets provided here are only adequate for models that do not include the indirect effects of aerosols, such as cloud nucleation. Models that include such effects may exhibit significant sensitivity to even slight changes in aerosol distribution and loading and we are not confident that the use of our Eocene datasets, given the uncertainties involved, would be scientifically sound.

Finally, we note that the ability to prognose aerosol distributions in long climate simulations (available in the latest atmospheric models, though at significant computational cost) will obviate the need for prescribed aerosol concentrations while also accounting for their indirect effects. Such models will see the emission sources of various aerosol species (e.g. deserts, volcanoes, regions of high marine productivity) become an important aspect of paleogeographic reconstructions.

GMDD
7, 529–562, 2014

2.6 River transport

River runoff in climate models is important primarily for the redistribution of fresh water to the oceans and can have significant implications for deep water formation (e.g. Bice et al., 1997). A global dataset of such information has not been constructed for the Eocene – though robust methodologies exist (Markwick and Valdes, 2004) – and as such topographic gradients are commonly used as a substitute for this boundary condition. Here we provide a dataset of vectors which follow the gradient of our Eocene topography and can be used to represent river runoff (Fig. 7). This dataset was created using scripts made available by the National Center for Atmospheric Research (Rosenbloom et al., 2011). Regions where vectors do not reach the ocean (i.e. internal basins) were manually corrected.

3 Summary and future work

We describe an openly available comprehensive set of Early Eocene climate model boundary conditions including topography, bathymetry, tidal dissipation, vegetation, aerosols and river transport. The resolution of most of these datasets is unprecedented and alleviates the undesirable step of downscaling lower resolution datasets to that of current generation models. This should therefore lead to improvements in model-data comparisons in regions of strong relief and facilitate high resolution global and regional model simulations. However, uncertainties in these data still exist. These are most pertinent in our tidal dissipation, aerosol and river runoff datasets. Advances in modelling may alleviate the former two while comprehensive compilation and analysis of geological data (e.g. Markwick and Valdes, 2004) can drastically improve the latter. A community effort to adopt consistent modelling methodologies will accelerate growth in our understanding of Eocene climates and help highlight the most pertinent shortcomings of the current generation of climate models.

GMDD
7, 529–562, 2014

Supplementary material related to this article is available online at http://www.geosci-model-dev-discuss.net/7/529/2014/gmdd-7-529-2014-supplement.zip.

Acknowledgements. We thank Douglas Wilson for providing us with the ANTscape topography. N. Herold, J. Buzan, A. Goldner and M. Huber are supported under *1049921-EAR: Collaborative Research: improved Cenozoic paleoelevation estimates for the Sierra Nevada, California: linking geodynamics with atmospheric dynamics*. M. Seton and R. D. Müller acknowledge support from Australian Research Council (ARC) grants DP0987713 and FL0992245, respectively. The tidal model simulations were funded by the Natural Environmental Research Council (grant NE/F014821/1) and the Climate Change Consortium for Wales (JAMG), and the National Science Foundation (grant 0927946-ATM to MH).

References

Backman, J., Duncan, R. A., Peterson, L. C., Baker, P. A., Baxter, A. N., Boersma, A., Cullen, J. L., Droxler, A. W., Fisk, M. R., Greenough, J. D., Hargraves, R. B., Hempel, P., Hobart, M. A., Hurley, M. T., Johnson, D. A., Macdonald, A. H., Mikkelsen, N., Okada, H., Rio, D., Robinson, S. G., Schneider, D., Swart, P. K., Tatsumi, Y., Vandamme, D., Vilks, G., and Vincent, E.: Site 707, ODP Ocean Drilling Program, 1988.

Barker, P. F. and Thomas, E.: Origin, signature and palaeoclimatic influence of the Antarctic Circumpolar Current, Earth-Sci. Rev., 66, 143–162, 2004.

Bar-Or, R., Erlick, C., and Gildor, H.: The role of dust in glacial–interglacial cycles, Quaternary Sci. Rev., 27, 201–208, doi:10.1016/j.quascirev.2007.10.015, 2008.

Barrera, E. B., Lohmann, J., and Kyger, C.: Strontium isotope and benthic foraminifer stable isotope results from Oligocene sediments at Site 803, ODP Ocean Drilling Program, 1993.

Barron, E. J.: Explanations of the Tertiary global cooling trend, Palaeogeogr. Palaeocl., 50, 45–61, 1985.

Barron, E. J.: Paleogeography and Climate, 180 Million Years to the Present, University of MIAMI, 1980.

GMDD

7, 529–562, 2014

Barron, E. J. and Peterson, W. H.: Mid-Cretaceous ocean circulation: results from model sensitivity studies, Paleoceanography, 5, 319–337, doi:10.1029/PA005i003p00319, 1990.
Barron, E. J. and Peterson, W. H.: The Cenozoic ocean circulation based on ocean General Circulation Model results, Palaeogeogr. Palaeocl., 83, 1–28, 1991.
Barron, E. J., Thompson, S. L., and Schneider, S. H.: An Ice-Free Cretaceous? Results from Climate Model Simulations, Science, 212, 501–508, doi:10.1126/science.212.4494.501, 1981.
Bice, K. L., Barron, E. J., and Peterson, W. H.: Continental runoff and early Cenozoic bottom-water sources, Geology, 25, 951–954, 1997.
Bice, K. L., Barron, E. J., and Peterson, W. H.: Reconstruction of realistic early Eocene paleobathymetry and ocean GCM sensitivity to specified basin configuration, Oxford Monographs on Geology and Geophysics, 39, 227–247, 1998.
Braconnot, P., Harrison, S. P., Kageyama, M., Bartlein, P. J., Masson-Delmotte, V., Abe-Ouchi, A., Otto-Bliesner, B., and Zhao, Y.: Evaluation of climate models using palaeoclimatic data, Nature Clim. Change, 2, 417–424, 2012.
Cramer, B. S., Miller, K. G., Barrett, P. J., and Wright, J. D.: Late Cretaceous–Neogene trends in deep ocean temperature and continental ice volume: Reconciling records of benthic foraminiferal geochemistry (δ^{18}O and Mg/Ca) with sea level history, J. Geophys. Res.-Ocean, 116, C12023, doi:10.1029/2011jc007255, 2011.
Crowley, C. W.: An atlas of Cenozoic climates, Masters of science in geology, The University of Texas, 2012.
Crowley, T. J. and Burke, K.: Tectonic Boundary Conditions for Climate Reconstructions, Oxford University Press, 1998.
Dalziel, I. W. D., Lawver, L. A., Norton, I. O., and Gahagan, L. M.: The Scotia Arc: genesis, evolution, global significance, Annu. Rev. Earth Pl. Sc., 41, 767–793, doi:10.1146/annurev-earth-050212-124155, 2013a.
Dalziel, I. W. D., Lawver, L. A., Pearce, J. A., Barker, P. F., Hastie, A. R., Barfod, D. N., Schenke, H.-W., and Davis, M. B.: A potential barrier to deep Antarctic circumpolar flow until the late Miocene?, Geology, 41, 947–950, doi:10.1130/g34352.1, 2013b.
DeConto, R. M., Galeotti, S., Pagani, M., Tracy, D., Schaefer, K., Zhang, T., Pollard, D., and Beerling, D. J.: Past extreme warming events linked to massive carbon release from thawing permafrost, Nature, 484, 87–91, 2012.
Donn, W. L. and Shaw, D. M.: Model of climate evolution based on continental drift and polar wandering, Geol. Soc. Am. Bull., 88, 390–396, 1977.

GMDD
7, 529–562, 2014

Dutton, J. F. and Barron, E. J.: Miocene to present vegetation changes; a possible piece of the Cenozoic cooling puzzle, Geology, 25, 39–41, 1997.
Egbert, G. D., Ray, R. D., and Bills, B. G.: Numerical modeling of the global semidiurnal tide in the present day and in the last glacial maximum, J. Geophys. Res.-Ocean, 109, C03003, doi:10.1029/2003jc001973, 2004.
Fisher, R. L., Bunce, E. T., Cernock, P. J., Clegg, D. C., Cronan, D. S., Damiani, V. V., Dmitriev, L. V., Kinsman, D. J., Roth, P. H., Thiede, J., and Vincent, E.: Site 237, DSDP Deep Sea Drilling Project, 1974.
Fuetterer, D. K.: Bioturbation and trace fossils in deep sea sediments of the Walvis Ridge, southeastern Atlantic, Leg 74, DSDP Deep Sea Drilling Project, IPOD International Phase of Ocean Drilling, 1984.
Garrett, C. and Kunze, E.: Internal Tide Generation in the Deep Ocean, Annu. Rev. Fluid Mech., 39, 57–87, doi:10.1146/annurev.fluid.39.050905.110227, 2007.
Gent, P. R., Danabasoglu, G., Donner, L. J., Holland, M. M., Hunke, E. C., Jayne, S. R., Lawrence, D. M., Neale, R. B., Rasch, P. J., Vertenstein, M., Worley, P. H., Yang, Z.-L., and Zhang, M.: The Community Climate System Model Version 4, J. Climate, 24, 4973–4991, doi:10.1175/2011jcli4083.1, 2011.
Goldner, A., Huber, M., and Caballero, R.: Does Antarctic glaciation cool the world?, Clim. Past, 9, 173–189, doi:10.5194/cp-9-173-2013, 2013.
Golonka, J.: Chapter 6 Phanerozoic palaeoenvironment and palaeolithofacies maps of the Arctic region, Geological Society, London, Memoirs, 35, 79–129, doi:10.1144/m35.6, 2011.
Green, J. A. M. and Huber, M.: Tidal dissipation in the early Eocene and implications for ocean mixing, Geophys. Res. Lett., 40, 2707–2713, doi:10.1002/grl.50510, 2013.
Harrison, S. P. and Prentice, C. I.: Climate and CO_2 controls on global vegetation distribution at the last glacial maximum: Analysis based on palaeovegetation data, biome modelling and palaeoclimate simulations, Glob. Change Biol., 9, 983–1004, 2003.
Heavens, N. G., Shields, C. A., and Mahowald, N. M.: A paleogeographic approach to aerosol prescription in simulations of deep time climate, J. Adv. Modeling Earth Syst., 4, M11002, doi:10.1029/2012ms000166, 2012.
Heinemann, M., Jungclaus, J. H., and Marotzke, J.: Warm Paleocene/Eocene climate as simulated in ECHAM5/MPI-OM, Clim. Past, 5, 785–802, doi:10.5194/cp-5-785-2009, 2009.

GMDD
7, 529–562, 2014

Henrot, A.-J., François, L., Favre, E., Butzin, M., Ouberdous, M., and Munhoven, G.: Effects of CO_2, continental distribution, topography and vegetation changes on the climate at the Middle Miocene: a model study, Clim. Past, 6, 675–694, doi:10.5194/cp-6-675-2010, 2010.

Herold, N., Seton, M., Müller, R. D., You, Y., and Huber, M.: Middle Miocene tectonic boundary conditions for use in climate models, Geochem. Geophy. Geosy., 9, Q10009, doi:10.1029/2008gc002046, 2008.

Herold, N., Huber, M., Müller, R. D., and Seton, M.: Modeling the Miocene climatic optimum: Ocean circulation, Paleoceanography, 27, PA1209, doi:10.1029/2010pa002041, 2012.

Hetzel, R., Dunkl, I., Haider, V., Strobl, M., von Eynatten, H., Ding, L., and Frei, D.: Peneplain formation in southern Tibet predates the India-Asia collision and plateau uplift, Geology, 39, 983–986, doi:10.1130/g32069.1, 2011.

Hill, D. J., Haywood, A. M., Valdes, P. J., Francis, J. E., Lunt, D. J., Wade, B. S., and Bowman, V. C.: Paleogeographic controls on the onset of the Antarctic circumpolar current, Geophys. Res. Lett., 2013GL057439, doi:10.1002/grl.50941, 2013.

Hollis, C. J., Taylor, K. W. R., Handley, L., Pancost, R. D., Huber, M., Creech, J. B., Hines, B. R., Crouch, E. M., Morgans, H. E. G., Crampton, J. S., Gibbs, S., Pearson, P. N., and Zachos, J. C.: Early Paleogene temperature history of the Southwest Pacific Ocean: reconciling proxies and models, Earth Planet. Sc. Lett., 349–350, 53–66, doi:10.1016/j.epsl.2012.06.024, 2012.

Huber, M. and Caballero, R.: The early Eocene equable climate problem revisited, Clim. Past, 7, 603–633, doi:10.5194/cp-7-603-2011, 2011.

Iakovleva, A. I., Brinkhuis, H., and Cavagnetto, C.: Late Palaeocene–Early Eocene dinoflagellate cysts from the Turgay Strait, Kazakhstan, correlations across ancient seaways, Palaeogeogr. Palaeocl., 172, 243–268, doi:10.1016/S0031-0182(01)00300-5, 2001.

Iturralde-Vinent, M. A.: Meso-Cenozoic Caribbean Paleogeography: implications for the historical biogeography of the region, Int. Geol. Rev., 48, 791–827, doi:10.2747/0020-6814.48.9.791, 2006.

Janecek, T. R. and Rea, D. K.: Eolian deposition in the northeast Pacific Ocean: Cenozoic history of atmospheric circulation, Geol. Soc. Am. Bull., 94, 730–738, doi:10.1130/0016-7606(1983)94<730:editnp>2.0.co;2, 1983.

Jayne, S. R., Laurent, L. C. S., and Gille, S. T.: Connections Between Ocean Bottom Topography and Earth's Climate, Oceanography, 17, 65–74, 2004.

GMDD
7, 529–562, 2014

Kaplan, J. O., Bigelow, N. H., Prentice, I. C., Harrison, S. P., Bartlein, P. J., Christensen, T. R., Cramer, W., Matveyeva, N. V., McGuire, A. D., Murray, D. F., Razzhivin, V. Y., Smith, B., Walker, D. A., Anderson, P. M., Andreev, A. A., Brubaker, L. B., Edwards, M. E., and Lozhkin, A. V.: Climate change and Arctic ecosystems: 2. Modeling, paleodata-model comparisons, and future projections, J. Geophys. Res., 108, 8171, doi:10.1029/2002jd002559, 2003.

Klocker, A., Prange, M., and Schulz, M.: Testing the influence of the Central American Seaway on orbitally forced Northern Hemisphere glaciation, Geophys. Res. Lett., 32, L03703, doi:10.1029/2004gl021564, 2005.

Kump, L. R. and Pollard, D.: Amplification of Cretaceous Warmth by Biological Cloud Feedbacks, Science, 320, p. 195, doi:10.1126/science.1153883, 2008.

Liu, Z., Pagani, M., Zinniker, D., DeConto, R., Huber, M., Brinkhuis, H., Shah, S. R., Leckie, R. M., and Pearson, A.: Global cooling during the Eocene-Oligocene climate transition, Science, 323, 1187–1190, doi:10.1126/science.1166368, 2009.

Lunt, D. J., Valdes, P. J., Haywood, A., and Rutt, I. C.: Closure of the Panama Seaway during the Pliocene: implications for climate and Northern Hemisphere glaciation, Clim. Dynam., 30, 1–18, 2008.

Lunt, D. J., Valdes, P. J., Jones, T. D., Ridgwell, A., Haywood, A. M., Schmidt, D. N., Marsh, R., and Maslin, M.: CO_2-driven ocean circulation changes as an amplifier of Paleocene-Eocene thermal maximum hydrate destabilization, Geology, 38, 875–878, doi:10.1130/g31184.1, 2010.

Lunt, D. J., Dunkley Jones, T., Heinemann, M., Huber, M., LeGrande, A., Winguth, A., Loptson, C., Marotzke, J., Roberts, C. D., Tindall, J., Valdes, P., and Winguth, C.: A model–data comparison for a multi-model ensemble of early Eocene atmosphere–ocean simulations: EoMIP, Clim. Past, 8, 1717–1736, doi:10.5194/cp-8-1717-2012, 2012.

Lyle, M.: Could early Cenozoic thermohaline circulation have warmed the poles?, Paleoceanography, 12, 161–167, 1997.

Mackensen, A. B. and William, A.: Paleogene benthic foraminifers from the southern Indian Ocean (Kerguelen Plateau), biostratigraphy and paleoecology, ODP Ocean Drilling Program, 1992.

Markwick, P. J.: The palaeogeographic and palaeoclimatic significance of climate proxies for data-model comparisons, in: Deep-Time Perspectives on Climate Change: Marrying the Sig-

GMDD
7, 529–562, 2014

nal from Computer Models and Biological Proxies, edited by: Williams, M., Haywood, A. M., Gregory, J., and Schmidt, D. N., Geological Society Special Publication, 251–312, 2007.
Markwick, P. J. and Valdes, P. J.: Palaeo-digital elevation models for use as boundary conditions in coupled ocean-atmosphere GCM experiments: a Maastrichtian (late Cretaceous) example, Palaeogeogr. Palaeocl., 213, 37–63, 2004.
Micheels, A., Bruch, A. A., Uhl, D., Utescher, T., and Mosbrugger, V.: A Late Miocene climate model simulation with ECHAM4/ML and its quantitative validation with terrestrial proxy data, Palaeogeogr. Palaeocl., 253, 251–270, 2007.
Mix, H. T., Mulch, A., Kent-Corson, M. L., and Chamberlain, C. P.: Cenozoic migration of topography in the North American Cordillera, Geology, 39, 87–90, doi:10.1130/g31450.1, 2011.
Molnar, P.: Closing of the Central American Seaway and the Ice Age: a critical review, Paleoceanography, 23, PA2201, doi:10.1029/2007pa001574, 2008.
Molnar, P., Boos, W. R., and Battisti, D. S.: Orographic controls on climate and paleoclimate of Asia: thermal and mechanical roles for the Tibetan Plateau, Annu. Rev. Earth Pl. Sc., 38, 77–102, doi:10.1146/annurev-earth-040809-152456, 2010.
Morley, R. J.: Cretaceous and Tertiary climate change and the past distribution of megathermal rainforests, in: Tropical Rainforest Responses to Climatic Change, Springer Praxis Books, Springer Berlin Heidelberg, 1–31, 2007.
Müller, R. D., Sdrolias, M., Gaina, C., and Roest, W. R.: Age, spreading rates, and spreading asymmetry of the world's ocean crust, Geochem. Geophy. Geosy., 9, Q04006, doi:10.1029/2007gc001743, 2008a.
Müller, R. D., Sdrolias, M., Gaina, C., Steinberger, B., and Heine, C.: Long-Term Sea-Level Fluctuations Driven by Ocean Basin Dynamics, Science, 319, 1357–1362, 2008b.
Neale, R. B., Richter, J. H., Conley, A. J., Park, S., Lauritzen, P. H., Gettelman, A., Williamson, D. L., Vavrus, S. J., Taylor, M. A., and Collins, W. D.: Description of the NCAR Community Atmosphere Model (CAM 4.0), 2010.
Otto-Bliesner, B. L. and Upchurch, G. R.: Vegetation-induced warming of high-latitude regions during the Late Cretaceous period, Nature, 385, 804–807, 1997.
Perch-Nielsen, K. S. P. R., Boersma, A., Carlson, R. L., Dinkelman, M. G., Fodor, R. V., Kumar, N., McCoy, F., Thiede, J., Zimmerman, H. B.: Site 357, Rio Grande Rise, DSDP Deep Sea Drilling Project, 1977.

GMDD
7, 529–562, 2014

Phillips, J. D. and Forsyth, D.: Plate tectonics, paleomagnetism, and the opening of the Atlantic, Geol. Soc. Am. Bull., 83, 1579–1600, doi:10.1130/0016-7606(1972)83[1579:ptpato]2.0.co;2, 1972.
Polzin, K. L., Toole, J. M., Ledwell, J. R., and Schmitt, R. W.: Spatial variability of turbulent mixing in the abyssal ocean, Science, 276, 93–96, doi:10.1126/science.276.5309.93, 1997.
Roberts, C. D., LeGrande, A. N., and Tripati, A. K.: Climate sensitivity to Arctic seaway restriction during the early Paleogene, Earth Planet. Sc. Lett., 286, 576–585, doi:10.1016/j.epsl.2009.07.026, 2009.
Rosenbloom, N., Shields, C., Brady, E. C., Levis, S., and Yeager, S. G.: Using CCSM3 for Paleoclimate Applications NATIONAL CENTER FOR ATMOSPHERIC RESEARCH, 2011.
Scher, H. D. and Martin, E. E.: Timing and climatic consequences of the opening of drake passage, Science, 312, 428–430, doi:10.1126/science.1120044, 2006.
Schlich, R.: Sites 246 and 247, DSDP Deep Sea Drilling Project, 1974.
Schubert, G. and Sandwell, D.: Crustal volumes of the continents and of oceanic and continental submarine plateaus, Earth Planet. Sc. Lett., 92, 234–246, 1989.
Scotese, C. R. and Golonka, J.: Paleogeographic Atlas, PALEOMAP Progress Report 20–0692, Department of Geology, University of Texas, Arlington, 34, 1992.
Sessa, J. A., Ivany, L. C., Schlossnagle, T. H., Samson, S. D., and Schellenberg, S. A.: The fidelity of oxygen and strontium isotope values from shallow shelf settings: Implications for temperature and age reconstructions, Palaeogeogr. Palaeocl., 342–343, 27–39, doi:10.1016/j.palaeo.2012.04.021, 2012.
Sewall, J. O. and Sloan, L. C.: Come a little bit closer: A high-resolution climate study of the early Paleogene Laramide foreland, Geology, 34, 81–84, doi:10.1130/g22177.1, 2006.
Sewall, J. O., Sloan, L. C., Huber, M., and Wing, S.: Climate sensitivity to changes in land surface characteristics, Global Planet. Change, 26, 445–465, 2000.
Shellito, C. J. and Sloan, L. C.: Reconstructing a lost Eocene Paradise, Part II: On the utility of dynamic global vegetation models in pre-Quaternary climate studies, Global Planet. Change, 50, 18–32, 2006a.
Shellito, C. J. and Sloan, L. C.: Reconstructing a lost Eocene paradise: Part I. Simulating the change in global floral distribution at the initial Eocene thermal maximum, Global Planet. Change, 50, 1–17, 2006b.
Shellito, C. J., Sloan, L. C., and Huber, M.: Climate model sensitivity to atmospheric CO_2 levels in the Early-Middle Paleogene, Palaeogeogr. Palaeocl., 193, 113–123, 2003.

GMDD
7, 529–562, 2014

Shellito, C. J., Lamarque, J.-F., and Sloan, L. C.: Early Eocene Arctic climate sensitivity to pCO_2 and basin geography, Geophys. Res. Lett., 36, L09707, doi:10.1029/2009gl037248, 2009.
Simmons, H. L., Jayne, S. R., Laurent, L. C. S., and Weaver, A. J.: Tidally driven mixing in a numerical model of the ocean general circulation, Ocean Model., 6, 245–263, doi:10.1016/S1463-5003(03)00011-8, 2004.
Sloan, L. C.: Equable climates during the early Eocene, significance of regional paleogeography for North American climate, Geology, 22, 881–884, 1994.
Sloan, L. C. and Rea, D. K.: Atmospheric carbon dioxide and early Eocene climate: A general circulation modeling sensitivity study, Palaeogeogr. Palaeocl., 119, 275–292, 1996.
Stein, C. A. and Stein, S.: A model for the global variation in oceanic depth and heat flow with lithospheric age, Nature, 359, 123–129, 1992.
Stickley, C. E., Brinkhuis, H., Schellenberg, S. A., Sluijs, A., Röhl, U., Fuller, M., Grauert, M., Huber, M., Warnaar, J., and Williams, G. L.: Timing and nature of the deepening of the Tasmanian Gateway, Paleoceanography, 19, PA4027, doi:10.1029/2004pa001022, 2004.
Stock, G. M., Anderson, R. S., and Finkel, R. C.: Pace of landscape evolution in the Sierra Nevada, California, revealed by cosmogenic dating of cave sediments, Geology, 32, 193–196, doi:10.1130/g20197.1, 2004.
Stocker, T., Qin, D., and Platner, G.: Climate Change 2013: The Physical Science Basis, Working Group I Contribution to the Fifth Assessment Report of the Intergovernmental Panel on Climate Change, Summary for Policymakers (IPCC, 2013), 2013.
Strömberg, C. A. E.: Evolution of Grasses and Grassland Ecosystems, Annu. Rev. Earth Pl. Sc., 39, 517–544, doi:10.1146/annurev-earth-040809-152402, 2011.
Torsvik, T. H., Carlos, D., Mosar, J., Cocks, L. R. M., and Malme, T. N.: Global reconstructions and North Atlantic paleogeography 440 Ma to recent, BATLAS – Mid Norway plate reconstruction atlas with global and Atlantic perspectives, 18–39, 2002.
Utescher, T. and Mosbrugger, V.: Eocene vegetation patterns reconstructed from plant diversity – a global perspective, Palaeogeogr. Palaeocl., 247, 243–271, doi:10.1016/j.palaeo.2006.10.022, 2007.
Vincent, E., Gibson, J. M., and Brun, L.: Paleocene and early Eocene microfacies, benthonic foraminifera, and paleobathymetry of Deep Sea Drilling Project sites 236 and 237, western Indian Ocean, DSDP Deep Sea Drilling Project, 1974.
Vinogradov, A. P.: Atlas Litologo-paleogeograficheskikh Kart SSSR: Atlas of the Lithological-paleogeographical Maps of the USSR, Glavnoe Upravlenie Geodezii I Kartografii, 1968.

GMDD
7, 529–562, 2014

Wakabayashi, J. and Sawyer, T. L.: Stream incision, tectonics, uplift, and evolution of topography of the Sierra Nevada, California, J. Geol., 109, 539–562, 2001.
Whittaker, J. M., Goncharov, A., Williams, S. E., Müller, R. D., and Leitchenkov, G.: Global sediment thickness data set updated for the Australian-Antarctic Southern Ocean, Geochem. Geophy. Geosy., 14, 3297–3305, doi:10.1002/ggge.20181, 2013.
Wilson, D. S., Jamieson, S. S. R., Barrett, P. J., Leitchenkov, G., Gohl, K., and Larter, R. D.: Antarctic topography at the Eocene–Oligocene boundary, Palaeogeogr. Palaeocl., 335–336, 24–34, doi:10.1016/j.palaeo.2011.05.028, 2012.
Winguth, A., Shellito, C., Shields, C., and Winguth, C.: Climate response at the Paleocene–Eocene thermal maximum to greenhouse gas forcing – a model Study with CCSM3, J. Climate, 23, 2562–2584, doi:10.1175/2009jcli3113.1, 2009.
Wohlfahrt, J., Harrison, S., Braconnot, P., Hewitt, C., Kitoh, A., Mikolajewicz, U., Otto-Bliesner, B., and Weber, S.: Evaluation of coupled ocean–atmosphere simulations of the mid-Holocene using palaeovegetation data from the Northern Hemisphere extratropics, Clim. Dynam., 31, 871–890, doi:10.1007/s00382-008-0415-5, 2008.
Wolfe, J. A.: Distribution of major vegetational types during the Tertiary, in: Geophysical Monograph, edited by: Sundquist, E. T. and Broecker, W. S., American Geophysical Union, Washington, DC, 357–375, 1985.
Zachos, J. C., Röhl, U., Schellenberg, S. A., Sluijs, A., Hodell, D. A., Kelly, D. C., Thomas, E., Nicolo, M., Raffi, I., Lourens, L. J., McCarren, H., and Kroon, D.: Rapid Acidification of the Ocean During the Paleocene-Eocene Thermal Maximum, Science, 308, 1611–1615, doi:10.1126/science.1109004, 2005.
Zhang, X., Prange, M., Steph, S., Butzin, M., Krebs, U., Lunt, D. J., Nisancioglu, K. H., Park, W., Schmittner, A., Schneider, B., and Schulz, M.: Changes in equatorial Pacific thermocline depth in response to Panamanian seaway closure: Insights from a multi-model study, Earth Planet. Sc. Lett., 317–318, 76–84, doi:10.1016/j.epsl.2011.11.028, 2012.
Ziegler, A. M., Scotese, C. R., and Barrett, S. F.: Mesozoic and Cenozoic Paleogeographic Maps, in: Tidal Friction and the Earth's Rotation II, edited by: Brosche, P., and Sündermann, J., Springer Berlin Heidelberg, 240–252, 1982.
Ziegler, A. M., Rowley, D. B., Lottes, A. L., Sahagian, D. L., Hulver, M. L., and Gierlowski, T. C.: Paleogeographic interpretation: with an example from the mid-cretaceous, Annu. Rev. Earth Pl. Sc., 13, 385–428, doi:10.1146/annurev.ea.13.050185.002125, 1985.

GMDD
7, 529–562, 2014

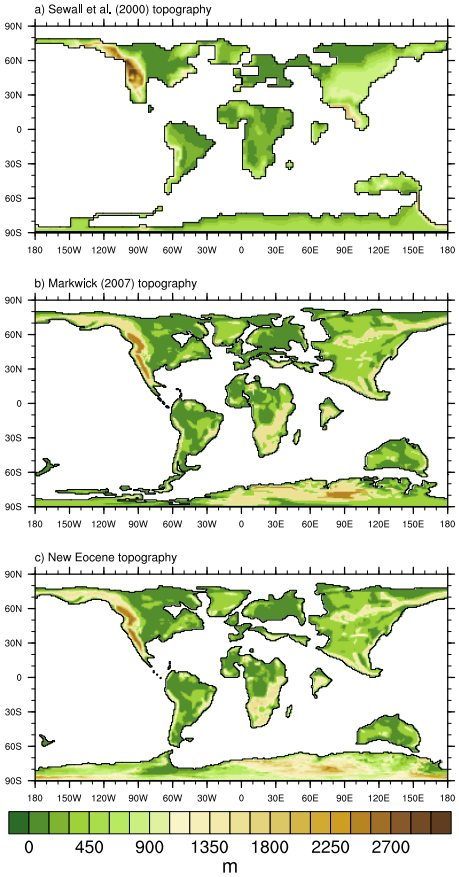

Fig. 1. Eocene topography from **(a)** Sewall et al. (2000) and **(b)** Markwick (2007), **(c)** our revised Eocene topography.

GMDD
7, 529–562, 2014

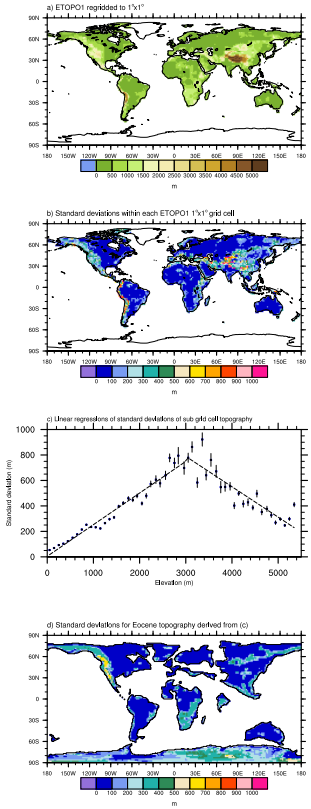

Fig. 2. Estimating the standard deviation of sub grid cell elevations for the Eocene. **(a)** ETOPO1 topography downscaled from its native $1' \times 1'$ resolution to $1^\circ \times 1^\circ$. **(b)** Standard deviation of $1' \times 1'$ elevations inside each $1^\circ \times 1^\circ$ grid cell. **(c)** Standard deviations from **(b)** area-weight averaged into 100 m bins and plotted against corresponding elevation. Standard error for each bin is plotted. Dotted lines represent linear regressions between sea-level and 3000 m, and 3000 m and 5500 m. **(d)** Linear regressions from **(c)** applied to Eocene topography (Fig. 1c). See text for details.

GMDD
7, 529–562, 2014

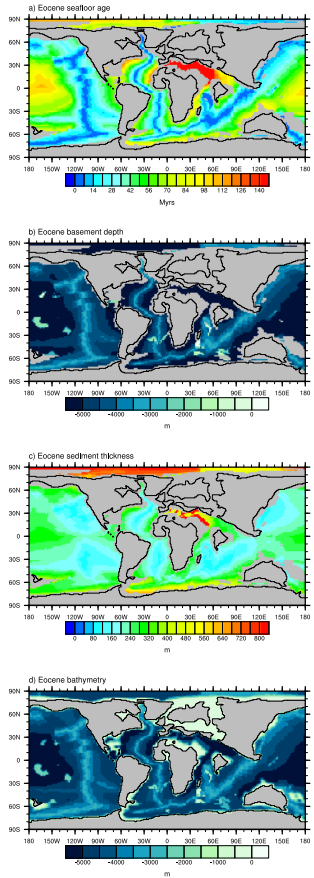

Fig. 3. 55 Ma **(a)** seafloor age, **(b)** basement depth, **(c)** sediment thickness and **(d)** final bathymetry. Black outlines indicate paleo shoreline.

GMDD
7, 529–562, 2014

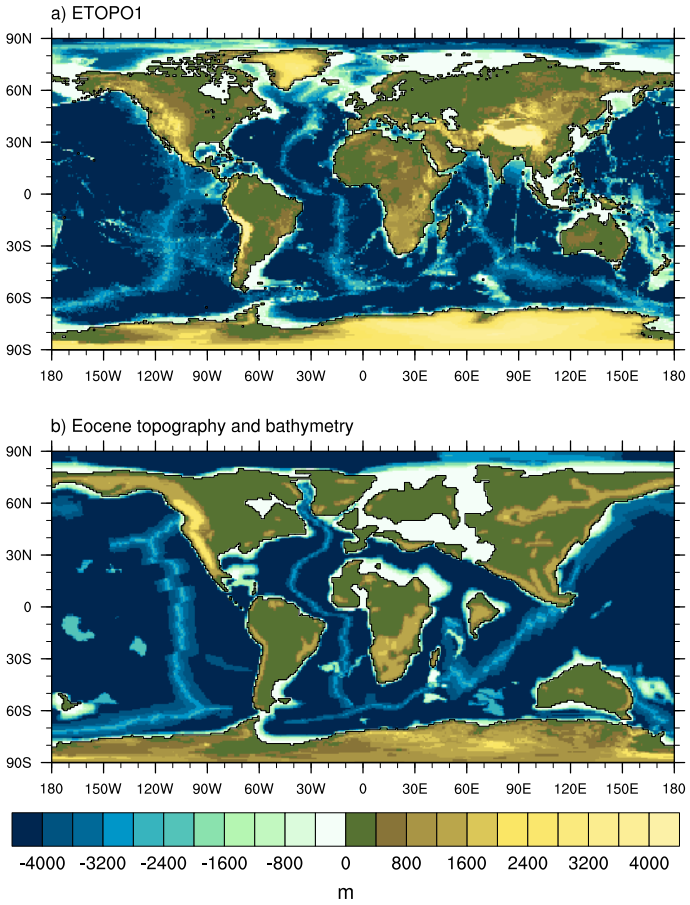

Fig. 4. (a) ETOPO1 topography and bathymetry, **(b)** new Eocene topography and bathymetry. Both at 1° × 1° resolution.

GMDD
7, 529–562, 2014

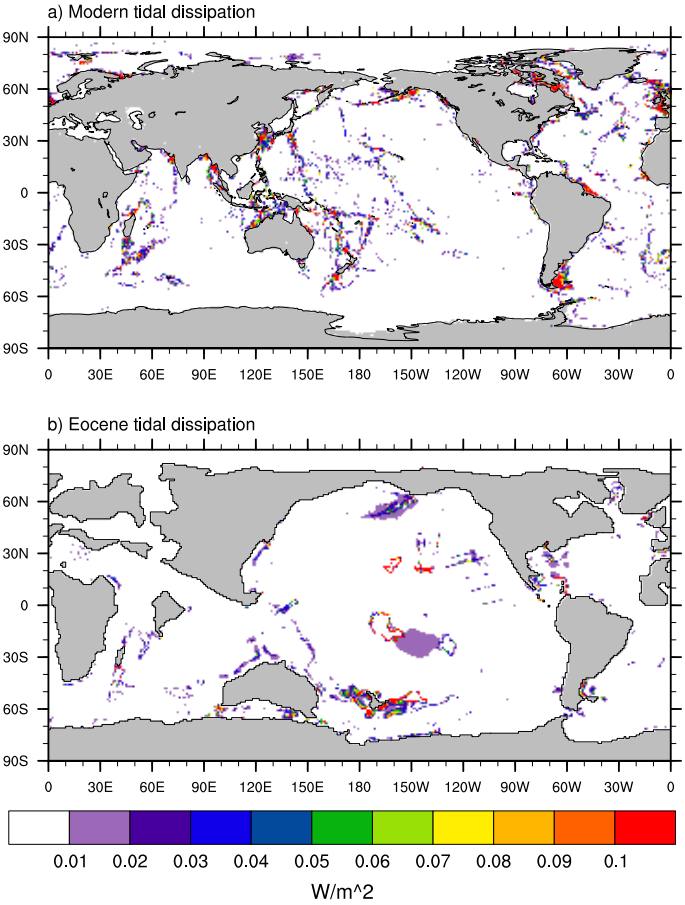

Fig. 5. (a) Modern and **(b)** Eocene simulated tidal dissipation (Green and Huber, 2013).

GMDD
7, 529–562, 2014

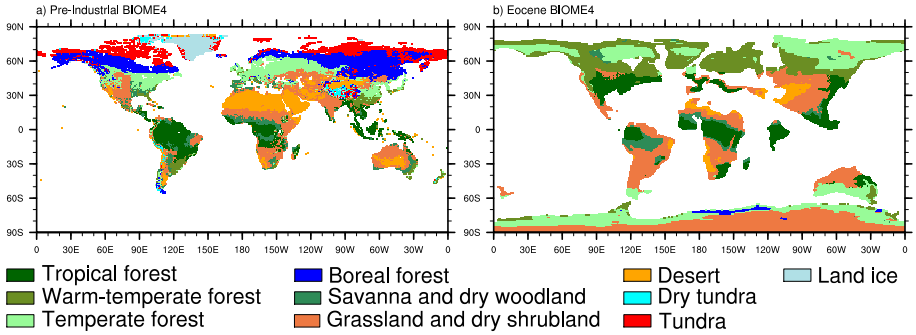

Fig. 6. (a) Pre-industrial and **(b)** Eocene vegetation simulated by BIOME4. The 27 biomes simulated by BIOME4 have been consolidated into 10 mega biomes following Harrison and Prentice (2003).

GMDD
7, 529–562, 2014

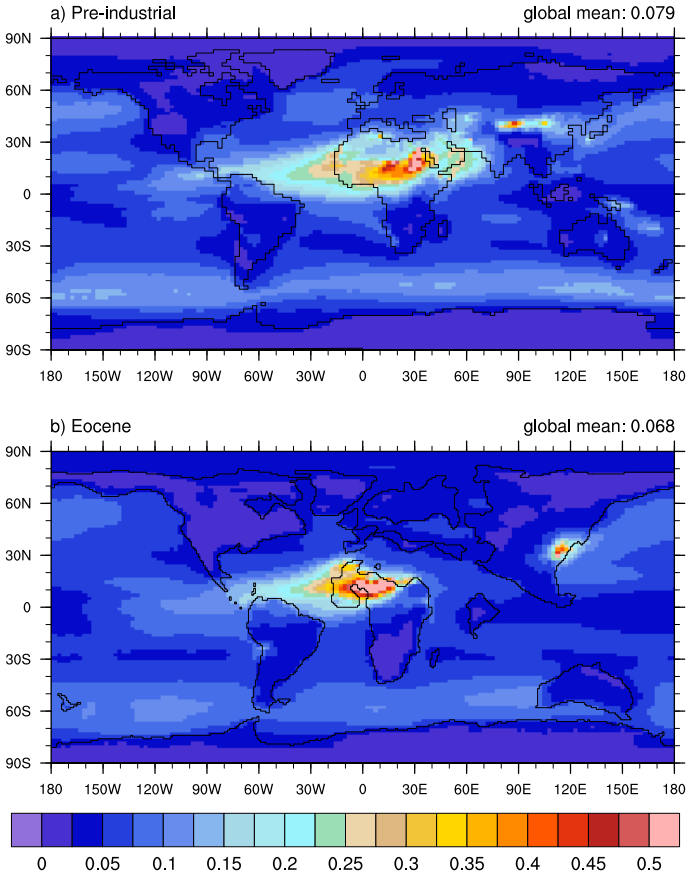

Fig. 7. (a) Pre-industrial and **(b)** Eocene aerosol optical depth (unitless) simulated by the Community Atmosphere Model 4.

GMDD
7, 529–562, 2014

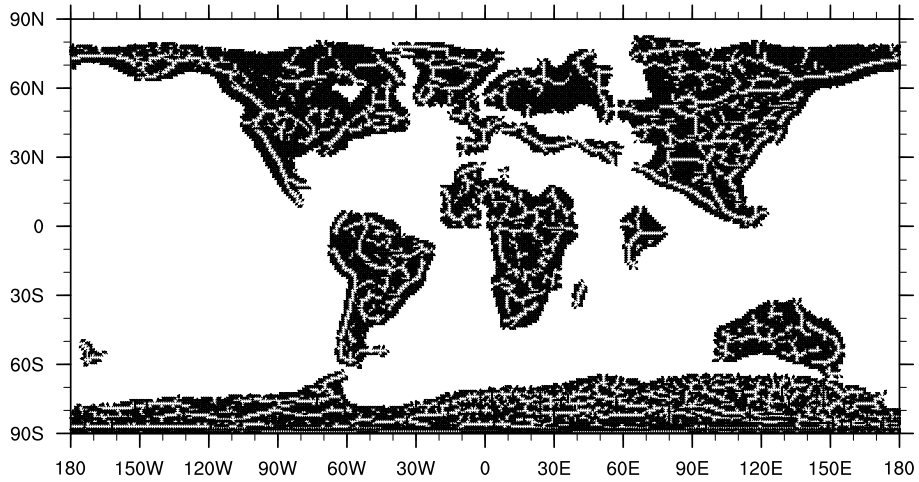

Fig. 8. Eocene river runoff directions.

GMDD
7, 529–562, 2014